energies

Article

Heat Transfer and Flow of a Gel Fuel in Corrugated Channels

Hao Zhou [1], Feng Feng [1], Qin-Liu Cao [2], Changsheng Zhou [1], Wei-Tao Wu [1] and Mehrdad Massoudi [3,*]

1 School of Mechanical Engineering, Nanjing University of Science & Technology, Nanjing 210094, China
2 Shanghai Xinli Power Equipment Institute, China Aerospace Science and Technology Corporation, Shanghai 201109, China
3 U.S. Department of Energy, National Energy Technology Laboratory (NETL), 626 Cochrans Mill Road, Pittsburgh, PA 15236, USA
* Correspondence: mehrdad.massoudi@netl.doe.gov

Abstract: For propulsion systems using gel fuels, reducing the gel fuel viscosity is essential for achieving better atomization and combustion. In this paper, we investigate the flow and heat transfer in a water-gel with a temperature and shear dependent viscosity. We consider several different channels, mimicking the transport of gelled fuels in propulsion systems, and we also look at corrugation, which is a way of enhancing fluid mixing and thus improving the heat transfer characteristics. The rheological parameters in the constitutive model of the gel are fitted with experimental data. The influence of different corrugation profiles, corrugation configuration parameters and the Reynolds number on the mean apparent viscosity and the pressure drop are investigated. It was found that the flow recirculation formed in the valley of the corrugations enhances the heat transfer and thus the temperature of the main flow. We also noticed an increase in the pressure drop due to the stronger viscous dissipation. Furthermore, it was observed that the sinusoidal corrugation can achieve lower viscosity with a lower pressure drop compared with triangular and trapezoidal corrugations. A shorter wavelength and a deeper wave amplitude of the corrugation seemed to be better for reducing the gel fuel viscosity, while we must consider the adverse consequence of increased pressure drop. A larger Reynolds number was helpful for both lowering the pressure drop and for reducing the viscosity. In addition, compared with a smooth straight pipe, a Y-shape corrugated channel with a constant inlet velocity reduced the mean apparent viscosity by 70.8%, and this value increased to 72.6% by further applying a pulsed inlet velocity, which can greatly enhance the gel fuel atomization and thus improve the combustion efficiency.

Keywords: non-Newtonian fluid; gel fuels; viscosity reduction; wall corrugation; CFD; heat transfer enhancement

Citation: Zhou, H.; Feng, F.; Cao, Q.-L.; Zhou, C.; Wu, W.-T.; Massoudi, M. Heat Transfer and Flow of a Gel Fuel in Corrugated Channels. *Energies* **2022**, *15*, 7287. https://doi.org/10.3390/en15197287

Academic Editor: Gianpiero Colangelo

Received: 2 September 2022
Accepted: 28 September 2022
Published: 4 October 2022

1. Introduction

Gel fuel is one of the better options to meet the requirement of high performance and safety for an aerospace propulsion system [1]. Gel fuel is a new kind of propellant with special rheological properties, which is formed by adding gellants into the liquid fuel [2–4]. The network structure formed between the base fuel and the gellant makes the gel fuel behave like a solid fuel at rest. It can flow like a liquid when subjected to shear forces. Therefore, the gel fuel combines the advantages of solid fuel and liquid fuel, and it has promising applications in propulsion system of rocket and ramjet [1,4]. However, after adding the gellants, the viscosity of the fuel increases, especially at lower shear rates, and it is known that a higher viscosity will lower the efficiency of fuel atomization and combustion [5–7]. Finding methods to effectively reduce the viscosity of the gel fuel during the transport process is an important aspect for propulsion system using gel fuel.

It has been observed that the shear-thinning phenomena, which means that the viscosity of the gel fuel can be reduced with an increase in the shear rate, is one of the most important mechanical properties of the gel fuel. The power-law model and the Carreau type model are the most used constitutive relations to describe the shear-thinning aspects of non-Newtonian fluids [8–10]. Natan et al. [11–13] numerically studied the flow of a power-law gel in converging pipes. The distributions and the variation of the velocity, the pressure drop and the viscosity in pipelines with different geometries were investigated. Yoon et al. [14] fitted their results to a Carreau-Yasuda type model. When the gel flowed through a plain-orifice atomizer, unsteady conditions were observed due to the high injection velocity. Cao et al. [15] measured the constitutive parameters for a water-HPC gel and fitted their experimental data with a Carreau-Yasuda model. The results suggested that the viscosity reduction and the pressure loss competed, and therefore, a balance or an optimum point must be considered for specific conditions.

Similar to many polymeric and non-Newtonian fluids [16,17], the viscosity of the gel fuel is also affected by temperature, where a higher temperature can lead to a lower viscosity. Shin and Cho [18] investigated flow and heat transfer of a temperature and shear dependent non-Newtonian fluid in a rectangular duct. Their results showed that the heat transfer was increased by 70–300% due to the increase of the velocity gradient (shear rate) near the wall, which was attributed to the combined effect of temperature dependence and shear-thinning effects in the viscosity. Rahimi et al. [19,20] measured gel fuel's viscosity under different shear rates and temperatures, and they fitted the parameters of the power-law model with temperature and gellant fraction. Cao et al. [21] studied the flow and heat transfer of a gel in straight pipes and typical injectors where the walls of the channel are heated. They found that when the gel was fully heated in a long pipe, the mean viscosity and the pressure drop at the outlet were significantly reduced. If the length of the pipe is 'shorter,' which is the case in real propulsion systems, the pressure drop can still be reduced effectively, while the viscosity reduction can be more complicated as heat cannot be effectively transferred to the main flow; this causes a high viscosity gel plug to be formed in the center of the pipe.

According to Cao et al. [21], simply heating the pipe walls (applying a constant temperature or a constant heat flux) is not necessarily an effective way of reducing the mean viscosity of the gel. In thermal engineering, corrugation is a commonly used heat transfer enhancement configuration [22]. In this scheme, the diameter of the pipe changes, causing an enhancement in the fluid motion and mixing. Hong et al. [23] designed a wavy corrugated tube by employing multi-longitudinal vortices. They found that the wavy corrugated tube exhibited excellent heat transfer rate and thermal performance evaluation criterion (PEC) when compared with the smooth tube. Akbarzadeh et al. [24] studied the entropy production and the thermo-hydraulic performance of wavy channels with three corrugated profiles. Due to the high performance and low entropy production, a sinusoidal corrugation was recommended. Wang et al. [25] numerically investigated the effect of swirl and spiral flow on the pressure drop and the enhanced heat transfer in internal, transversal and helical corrugated tubes. They found that heat transfer enhancement could be attributed to the improvements due to convection and the nature of the turbulent flow. Shubham et al. [26] numerically studied the thermo-hydraulic transport characteristics of non-Newtonian fluids in corrugated channels. Their results indicated that the enhancement in heat transfer was not significant for a smaller amplitude of the wall waviness. Afrouzi et al. [27] studied pulsating flow of non-Newtonian fluids in a corrugated channel. It was mentioned that the skin friction factor was directly proportional to the power-law index and indirectly related to the Reynolds number *Re*. Hilo et al. [28] numerically studied the turbulent fluid flow and heat transfer through backward-facing step channels with various corrugated walls, and they found that the heat transfer was significantly enhanced.

The corrugated channels have been applied widely for enhancing the heat transfer efficiency, while according to the best of our knowledge, the viscosity reduction due to temperature-sensitive gel fuel using corrugated channels has not been reported yet. In this paper, we use the corrugation configurations, which are able to significantly enhance the fluid convection and the heat transfer. We use the corrugation coefficient to determine the effects of viscosity reduction to the temperature and the shear dependent gel fuel viscosity when transported in a pipe with a heated wall. In Section 2, we discuss the mathematical model by presenting the governing equations and the constitutive relations. The fitting of the experimentally measured constitutive parameters is also mentioned. In Section 3, we introduce the geometry of the studied problems and the mesh independence study. In Section 4, we present and discuss the numerical results.

2. Methods

2.1. Mathematical Model

In this work, the gel fuel is considered to be a non-Newtonian fluid, and its apparent viscosity depends on the shear rate and the temperature. We do not consider any chemical or electromagnetic effects. The governing equations are the conservation equations for mass, momentum, and the energy equation, which are shown below [29,30].

2.1.1. Governing Equations

Conservation of mass:

$$\frac{\partial \rho}{\partial t} + \operatorname{div}(\rho \mathbf{v}) = 0 \tag{1}$$

where $\partial/\partial t$ is the partial derivative with respect to time, div is the divergence operator, $\mathbf{v}$ is the velocity vector and ρ is the density of the fluid. If the fluid is assumed to be incompressible, then it can only undergo isochoric (i.e., volume preserving) motions, $\operatorname{div}\mathbf{v} = 0$

Conservation of momentum:

$$\rho \frac{d\mathbf{v}}{dt} = \operatorname{div}\mathbf{T} + \rho \mathbf{b} \tag{2}$$

where d/dt is the total time derivative given by $d(.)/dt = \partial(.)/\partial t + [\operatorname{grad}(.)]\mathbf{v}$ and grad is the gradient operator, $\mathbf{T}$ is the Cauchy stress tensor and $\mathbf{b}$ is the body force which is ignored here.

Conservation of energy:

$$\frac{de}{dt} = \mathbf{T} : \mathbf{L} - \operatorname{div}\mathbf{q} + \rho r \tag{3}$$

where e is the internal energy density, $\mathbf{L}$ is the velocity gradient, $\mathbf{q}$ is the heat flux vector and r is the specific radiant energy, which is neglected in this study. $\mathbf{T} : \mathbf{L}$ represents the viscous dissipation, and $\mathbf{q}$ represents the heat conduction [30].

In this paper, the governing equations are discretized by the finite volume method with the PISO algorithm for velocity-pressure coupling. The discretization schemes of the conservation equations are shown in Table 1.

Table 1. Discretization schemes of the conservation.

Conservation Equation	Discretization
Gradient	Gauss linear
convection	bounded Gauss upwind
Diffusion	Gauss linear corrected
Time	Euler

2.1.2. Constitutive Equations

Looking at the above equations, we can see that we need constitutive relations for the stress tensor, heat flux vector, radiation and the internal energy. In this problem, we ignore the effects of radiation, and we assume $e = \rho\varepsilon$, where $\varepsilon = C_p\theta$ and C_p is the heat capacity. For the heat flux vector, we assume the classical theory of Fourier heat conduction [31]:

$$\mathbf{q} = -k \operatorname{grad} \theta \tag{4}$$

where k is the thermal conductivity of the gel fuel. In general, the thermal conductivity can be a function of temperature, volume fraction, etc. According to the available experimental data [32], changing the fraction of the gellant in the gel, the thermal conductivity changes moderately, and therefore, the value of k does not change much. Thus, the value of k can be assumed to be the same as the thermal conductivity of water.

For the stress tensor of the gel fuel, we assume that gel is a non-Newtonian fluid. These fluids often show some special non-linear characteristics. For example, some non-Newtonian fluids have yield stress or exhibit viscoelasticity, thixotropy, etc., and their viscosity can depend on shear rate, temperature and even pressure [33]. In this paper, we assume that the viscosity of the gel depends on both the shear rate and the temperature. The stress tensor of the gel is given by a non-Newtonian model:

$$\mathbf{T} = -p\mathbf{I} + 2\eta(\Psi)\mathbf{D} \tag{5}$$

where $\mathbf{I}$ is the identity tensor and $\mathbf{D}$ is the symmetric part of the velocity gradient $\mathbf{D} = 1/2\left[\text{grad } \mathbf{v} + (\text{grad } \mathbf{v})^T\right]$. For a generalized non-Newtonian fluid (GNF) [34], the shear viscosity $\eta(\Psi)$ can be a function of one or all of the following: (1) time, (2) shear rate, (3) concentration, (4) temperature, (5) pressure, (6) electric field, (7) magnetic field, etc. Thus, in general,

$$\eta(\Psi) = \eta(t, \pi, \theta, \varphi, p, \boldsymbol{E}, \boldsymbol{B}, \ldots) \tag{6}$$

where t is the time. π is some measure of the shear rate (for example, $\dot{\gamma} = \sqrt{2tr\mathbf{D}^2}$), where tr is the trace operator, θ is the temperature, φ is the concentration, p is the pressure, $\boldsymbol{E}$ is the electric field and $\boldsymbol{B}$ is the magnetic field. Of course, in many applications, the dependence of one or more of these can be dropped. One of the most widely used GNF models is the Carreau-Yasuda equation. According to [11,35], the gel can be treated as a Carreau-Yasuda type fluid. Thus, we assume:

$$\eta(\dot{\gamma}) = \eta_\infty + (\eta_0 - \eta_\infty)\left[1 + (\dot{\gamma}\lambda)^b\right]^{\frac{n-1}{b}} \tag{7}$$

where η_0 and η_∞ represent the viscosity when the shear rate approaches zero or infinity. The parameter $\dot{\gamma}$ is the shear rate. The parameter b controls the shape of the viscosity versus the shear rate curve during the initial descent curve. The parameter λ is the relaxation time, which is the time constant of a fluid in response to a change in the shear rate. The parameter n is a similar parameter to the exponential term in the power-law model, which controls the slope of the viscosity during the rapid change with shear rate.

For the temperature dependence of the viscosity, one of the most useful equations is the Reynolds viscosity model:

$$\eta(\theta) = \eta_0 e^{-M\theta} \tag{8}$$

where $M = \alpha(\theta_1 - \theta_0)$, where α is a constant. This viscosity expression was first proposed by Reynolds (1866) in his theory of lubrication, where he deduced an empirical formula based on the experimental results of the viscosity of olive oil at different temperatures; this expression is oftentimes used in lubrication and other engineering applications [36,37]. In addition to the Reynolds equation, in certain applications, the Vogel's model is used [38,39], where $\eta(\theta) = \eta_0 e^{\frac{a}{b+\theta}}$. In this paper, based on the Andrade-Eyring law [33], the viscosity relationship usually has an exponential form. Thus, we incorporate a Reynolds type model into the shear viscosity of the Carreau-Yasuda model and assume the following equation for the shear rate and the temperature dependent viscosity:

$$\eta(\theta, \dot{\gamma}) = \left\{\eta_\infty + (\eta_0 - \eta_\infty)\left[1 + (\dot{\gamma}\lambda)^b\right]^{\frac{n-1}{b}}\right\} exp^{c_1\theta + c_2} \tag{9}$$

where, c_1 and c_2 are the temperature indices. Note that the viscosity when the shear rate approaches zero or infinity at different temperatures should be $\eta_0 exp^{c_1\theta+c_2}$ and $\eta_\infty exp^{c_1\theta+c_2}$.

The material parameters in Equation (9) will be fitted to the experimental measurement in Section 2.2.

2.1.3. Expanded Form of the Governing Equations

Substituting Equations (5) and (9) into Equation (2), we obtaine a set of partial differential equations (PDEs), which need to be solved numerically. We built our PDEs solver using the libraries provided by OpenFOAM [40]. The dimensionless form of these PDEs are presented below:

$$\mathrm{div}^* \, \mathbf{V} = 0 \tag{10}$$

$$\frac{\partial \mathbf{V}}{\partial \tau} + \mathbf{V}\,(\mathrm{grad}^* \, \mathbf{V}) = -\mathrm{grad}^* \, P + \frac{1}{Re}\mathrm{div}^* \left(\frac{\eta(\theta, \dot{\gamma})}{\eta_r} \mathbf{D}^* \right) \tag{11}$$

$$\frac{\mathrm{d}\Theta}{\mathrm{d}\tau} + \mathbf{V}\,(\mathrm{grad}^* \, \Theta) = D_s \frac{\eta(\theta, \dot{\gamma})}{\eta_r} \mathbf{D}^* : \mathbf{L} + Le(\mathrm{div}^* \, (\mathrm{grad}^* \, \Theta)) \tag{12}$$

where the following non-dimensional parameters are defined:

$$Y = \frac{y}{L_r};\ X = \frac{x}{L_r};\ \mathbf{V} = \frac{\mathbf{v}}{v_0}; \tau = \frac{t v_0}{L_r}; \Theta = \frac{\theta - \theta_0}{\theta_1 - \theta_0}; \dot{\Gamma} = \frac{\dot{\gamma}}{\dot{\gamma}_r}; \Pi = \frac{\eta}{\eta_r}$$

$$P = \frac{p}{\rho v_0^2}; Re = \frac{\rho L_r v_0}{\eta_r}; D_s = \frac{\eta_r v_0}{\rho C_p(\theta_1 - \theta_0) L_r}; Le = \frac{k}{\rho C_p v_0 L_r} \tag{13}$$

$$\mathrm{div}^*(\cdot) = L_r \mathrm{div}(\cdot);\ \mathrm{grad}^*(\cdot) = L_r \mathrm{grad}(\cdot);\ \mathbf{D}^* = \mathrm{grad}^* \mathbf{V} + (\mathrm{grad}^* \mathbf{V})^T;$$

where L_r is the reference length, v_0 is the reference velocity, θ_1 and θ_0 are the reference temperatures and are set as 372 K and 298 K, and $\dot{\gamma}_r$ the reference shear rate, which is the mean shear rate of the cross-section. In this paper, η_r is the reference viscosity and Re is the Reynolds number. To determine whether the flow is laminar or turbulent, we further define a generalized Reynolds number as in Ref. [14]:

$$Re_{\mathrm{gen,CY}} = \frac{\rho \overline{u}}{\left[\left[1 + \left\{ \lambda \left(\frac{3n+1}{4n} \right) \frac{4\overline{u}}{R} \right\}^b \right]^{(n-1)/b} (\eta_0 - \eta_\infty) + \eta_\infty \right] \left(exp^{c_1 \theta + c_2} \right) \left(\frac{3n+1}{8nR} \right)} \tag{14}$$

where $\overline{u}$ is the mean velocity and R is radius of the pipe in the study.

2.2. Parameters in the Constitutive Equation

The shear rate and the temperature are two independent parameters which can affect the viscosity. A variable-controlling approach is adopted when obtaining experimental data: obtaining the viscosity at different shear rates with the temperature kept constant or obtaining the viscosity at different temperatures with the shear rate kept constant. The experimental data from Ref. [41] are used to fit the parameters in the constitutive model. It should be noticed that in the present paper, a water-gel is used to mimic the fuel gel. The experimental data and the curves predicted by the model are shown in Figure 1. The parameters in Equation (9) are $\eta_0 = 71.2713$ Pa·s, $\eta_\infty = 0.0271$ Pa·s, $\lambda = 0.1582$, b = 1.3814, $n = 0.3964$, $c_1 = -0.011$ (1/K), $c_2 = 0.0611$.

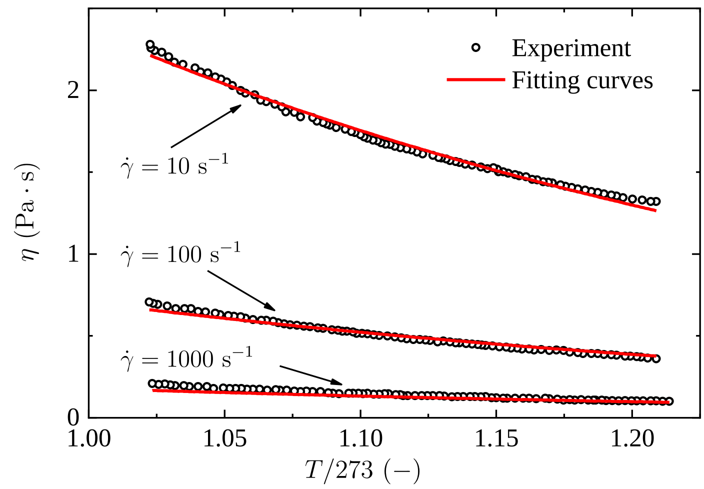

Figure 1. Experimental measurements and the model prediction of the viscosity of the water gel. The experimental data are from Ref. [41].

3. Problem Descriptions

There are several different types of corrugations which are used in real applications. Figure 2 shows the geometries of a channel with wall corrugation. The gel flows from left to right. The channel has three sections: the fully developed section, the test section and the exit section. The height of the channel is H. The lengths of three sections are $8H$, $12H$ and $4H$, respectively. In the test section, three different corrugation profiles are studied: sinusoidal, triangular, and trapezoidal. The triangular corrugation has the same spatial points to the sinusoidal corrugation at $k\pi$ and $k\pi + \pi/2$, and the trapezoidal corrugation is tangent to the sinusoidal corrugation at these points. These three corrugation profiles share the same wavelength (L_w) and wave amplitude (a).

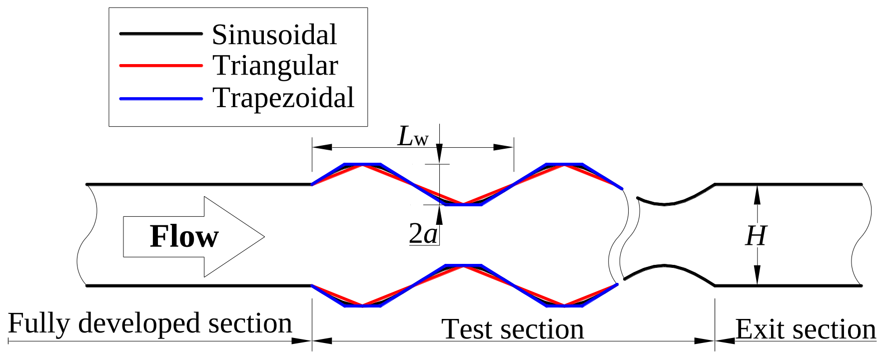

Figure 2. Geometries of the channel with wall corrugation. H is the channel height. The computational domain was divided in the fully developed section, the test section and the exit section, respectively. The lengths of these three sections were $8H$, $12H$ and $4H$. L_w is the wavelength, and a is the wave amplitude.

There are four boundary types used in this study: inlet, outlet, cold (unheated) wall and heated wall. The boundary condition at the inlet is a constant velocity with room temperature, which is 298 K. The walls of the fully developed section are cold (unheated) walls. The walls of the test section and the exit section are heated walls. The zero gradient condition is applied for the velocity and the temperature at the outlet. For the details of the boundary conditions, see Table 2. In addition, Table 3 lists the geometry and the flow parameters for the cases studied in this paper.

Table 2. Boundary conditions for the numerical simulation.

Boundary Type	Pressure	Velocity	Temperature
Cold Wall	Zero gradient	Fixed value (0)	Fixed value (298 K)
Heat wall	Zero gradient	Fixed value (0)	Fixed value (372 K)
Inlet	Zero gradient	Fixed value	Fixed value (298 K)
Outlet	Fixed value (0)	Zero gradient	Zero gradient

Table 3. Simulation conditions in this study.

Research Points	a	L_w	$Re_{\mathrm{gen,CY}}$
Corrugation profile	$1/5H$	$2H$	130
Wavelength	$1/5H$	$2H$, $2.4H$, $3H$, $4H$, $6H$	130
Wave amplitude	$1/20H$, $1/10H$, $3/20H$, $1/5H$	$2H$	130
Reynolds number	$1/5H$	$2H$	43, 130, 247, 390, 555

In this paper, we use sinusoidal bellows to verify mesh independence, where $a = 1/10H$, $L_{\mathrm{w}} = 2H$ and $Re_{\mathrm{gen,CY}} = 130$. The outlet average viscosity and the viscosity distribution are used as the determining criteria. The average viscosity at the outlet under different mesh numbers is shown in Table 4, and the viscosity distribution at the outlet is shown in Figure 3.

Table 4. Average viscosity at the outlet under different mesh numbers.

	Mesh Numbers	Average Viscosity (Pa·s)
Case1	12,000	0.18208
Case2	24,000	0.18559
Case3	48,000	0.18474
Case4	96,000	0.18768

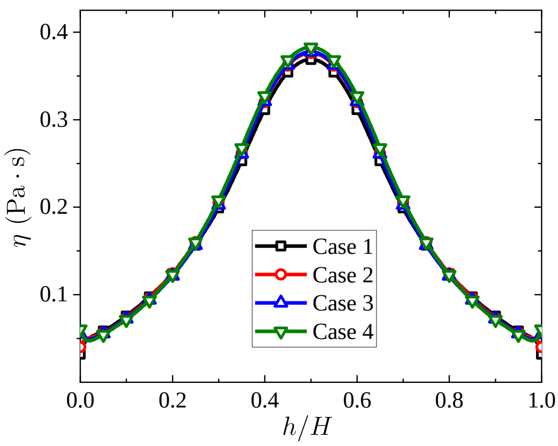

Figure 3. Average viscosity distribution at the outlet for different mesh numbers.

It can be seen that for different mesh numbers, the error between the calculated results is small. The maximum relative error of the average viscosity of the four tests is about 3%. Therefore, it can be seen that the results are independent of the grid size. A mesh number of 12,000 is used in the paper.

The following cases are used to verify the accuracy of the model:

First, we simplify the Carreau-Yasuda model (shown in Equation (9)) to a Newtonian fluid and ignore the temperature effects. That is, we assume $n = 1$, $\eta_\infty = 0, c_1 = 0$, $c_2 = 0$. Then, the Carreau-Yasuda model is simplified to the Newtonian fluid model, as shown in Equation (15):

$$\eta(\theta, \dot{\gamma}) = \eta_0 \tag{15}$$

We then use the simplified model to obtain an analytical solution to the Poiseuille flow. The analytical solution is shown in Equation (16):

$$u_x = \frac{1}{2\eta}\frac{\Delta p}{L}y(d-y) \tag{16}$$

where u_x is the velocity in the x-direction, η is the dynamic viscosity, $\frac{\Delta p}{L}$ is the pressure gradient, L is the pipe length and d is the pipe diameter. The values in the verification process are: $\eta = 1$ Pa·s, $\Delta p = 10^5$ Pa, $L = 120$ mm, $d = 5$ mm. Both the numerical and the analytical solutions are plotted in Figure 4.

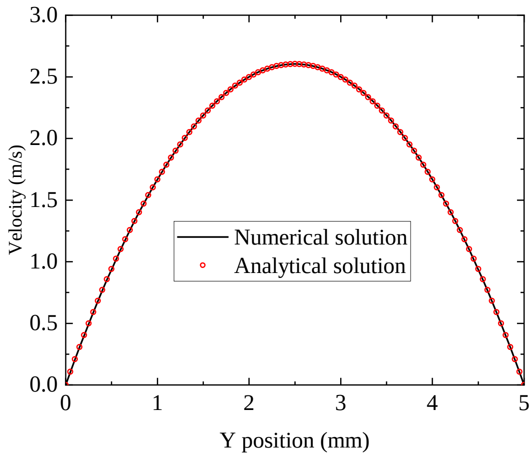

Figure 4. Comparison of the numerical and the analytical solutions of the Poiseuille flow.

As shown in Figure 4, the numerical results are very close to the analytical values.

For the second case, we use the back-step flow geometry and the results in [42] to validate our model. The geometry is shown in Figure 5. The parameters of the Carreau-Yasuda model are $\eta_\infty = 0.056$ Pa·s, $\eta_\infty = 0.0035$ Pa·s, $\lambda = 3.313$ $n = 0.0.3568$, $b = 2$, $c_1 = 0, c_1 = 0$. The initial conditions are consistent with those in [42]. For more details, please refer to [42]. Figure 6 shows the comparison of the numerical simulations for the velocity distribution at the outlet with the reference values in [42].

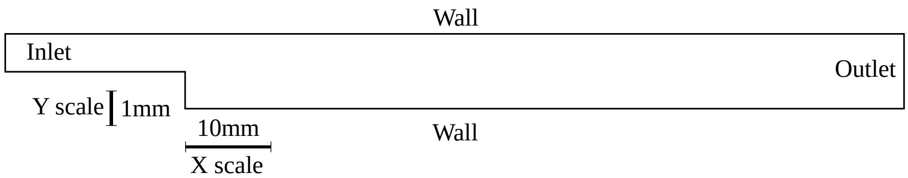

Figure 5. Geometry of the back-step flow used in Ref. [42].

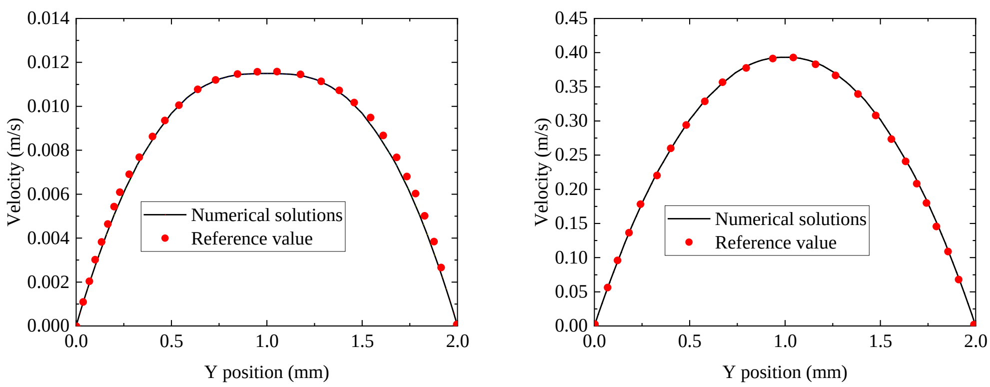

Figure 6. Comparison of the numerical simulation results and the reference value in Ref. [42].

As shown in Figure 6, the numerical results are very close to the values in [42]. Based on the observations shown in Figures 4 and 6, it can be assumed that the proposed numerical scheme is an accurate one.

4. Results and Discussion

For the transport systems using gel fuel, the main issues are pressure drop and viscosity. Our goal is to study the possibility of lowering the viscosity with a smaller pressure drop at the outlet of the transport pipe. In this study, we mainly focus on the results at the exit section. The position is located at $x/H = 20$. The dimensionless pressure drop is defined as:

$$\Delta P = \frac{\Delta p}{\rho v_0^2} \tag{17}$$

which has been mentioned in Equation (13). To obtain a better understanding of the effects of the corrugation configuration and the flow conditions, a mean apparent viscosity in a 2D channel is defined as in [15]:

$$\overline{\eta} = \frac{1}{H}\int \eta dh \tag{18}$$

For the 3D pipe case, the mean apparent viscosity has the form:

$$\overline{\eta} = \frac{1}{S}\int \eta ds \tag{19}$$

where S is the area of the cross section of the channel. The mean velocity, mean shear rate and mean temperature share the similar forms. In this section, the effect of corrugation profiles is investigated first, further determining the best corrugation for the further study. Then, we parametrically study the wavelength, the wave amplitude, and the Reynolds number. Finally, we investigate the viscosity reduction of the gel in a Y-shape channel formed by two corrugated channels with pulsed inlet velocity.

To evaluate the enhanced heat transfer characteristics of different pipes, the PEC evaluation method in [42] is used here. The specific definitions are:

$$Nu = \left.\frac{\partial T}{\partial n}\right|_w \cdot \frac{D}{T_w - T_f} \tag{20}$$

$$\overline{Nu} = \frac{1}{L_w}\int_0^{L_w} Nu ds \tag{21}$$

$$f = 2D \cdot \Delta p / \left(L\rho u^2\right) \tag{22}$$

$$\mathrm{PEC} = \left(\overline{Nu}/\overline{Nu_P}\right)/\left(f/f_P\right)^{1/3} \tag{23}$$

where n is the unit outward normal to the boundary surface, D is the diameter of the pipe, T_w is the wall temperature of the test section, T_f is the fluid temperature, Nu is the local Nusselt number, L_w is the wall length of the test section, $\overline{Nu}$ is the spatially averaged Nusselt number, Δp is the pressure drop of the test section. f is the friction factor, $\overline{Nu_P}$ and f_P are the corresponding values for the smooth pipe.

4.1. Effect of Corrugation Profiles

In this study, the mean velocity, the mean shear rate and the mean apparent viscosity of the cross section at the entrance of the test section of each corrugation are selected as the reference parameters and used to calculate the dimensionless numbers. The geometry and the flow conditions are listed in Table 3. The streamlines in the channels with different corrugation profiles in the last wave are shown in Figure 7. In all concavities, we can see some recirculation regions, which can enhance the mixing of the high-temperature fluid near the wall and the low-temperature fluid in the main flow. Furthermore, the sinusoidal corrugation has a similar size of recirculation region to triangular corrugation, and the trapezoidal corrugation has the biggest recirculation region.

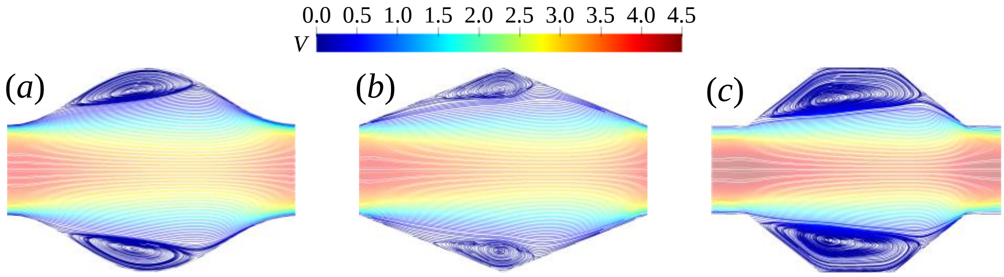

Figure 7. Streamlines in the last corrugation wave with (**a**) sinusoidal, (**b**) triangular and (**c**) trapezoidal profiles when $Re_{\mathrm{gen,CY}} = 130$.

Figure 8 shows the dimensionless velocity, the temperature, the shear rate and the viscosity in the transverse direction at the outlet of the test section for channels with different corrugation profiles and smooth channel. Figure 8a indicates that there is a large difference in the velocity profiles between the smooth and the corrugated channels. The velocity profile of the smooth channel is blunter, indicating a plug-type flow. For the corrugated channels, a velocity fluctuation near the wall is detected, which indicates the presence of a recirculation region. From Figure 8b, it can be observed that for the smooth channel, the temperature near the centerline is almost unaffected, while for the corrugated channels, the temperature of the main flow is higher than the temperature of the incoming flow. This implies that the corrugations have a significant effect on the heat convection enhancement. Among the three corrugation profiles, the trapezoidal corrugation performs the best because of the larger heating wall and the larger recirculation region. Figure 8c,d show the profiles of the dimensionless shear rate and the viscosity. For the smooth channel, near the wall, a lubrication layer with high temperature, high shear rate and low viscosity is formed. Near the center, a plug-type flow with a high viscosity can be observed. For the corrugated channel, due to the flow disturbance caused by the corrugation, the higher temperature fluid near the walls is transported to the main flow region and, as a result, the high viscosity plug flow near the channel center is diminished.

Table 5 lists the dimensionless pressure drop (ΔP) and the mean apparent viscosity ($\overline{\Pi}$) at the outlet of the test section for the corrugated channel and the smooth channel and the thermal performance evaluation criterion. Recall that ΔP is a measure of the dimensionless pressure drop between the two sides of the test section and $\overline{\Pi}$ is calculated based on the data shown in Figure 8d. The values of ΔP for the corrugated channels are more than three times larger when compared to the smooth channel, which is consistent with the conclusion of [24]. For different corrugation profiles, the trapezoidal corrugation has the highest ΔP because it has the largest recirculation region. The sharp corner of the triangular corrugation is a factor which can increase ΔP. Therefore, although the sinusoidal corrugation and the triangular have a similar size recirculation region, the sinusoidal corrugation has a lower ΔP. For the $\overline{\Pi}$, the corrugated channels have much lower values, and the sinusoidal corrugation performs the best. Taking both ΔP and $\overline{\Pi}$ into consideration, we choose the sinusoidal corrugation for the remainder of this study.

Table 5. The dimensionless pressure drop of the test section and the dimensionless mean apparent viscosity of the cross section at the outlet of the test section of the corrugated and smooth channels and thermal performance evaluation criterion.

	Sinusoidal	**Triangular**	**Trapezoidal**	**Smooth**
ΔP	3.34	4.24	5.65	1.03
$\overline{\Pi}$	0.31	0.49	0.34	1.72
PEC	1.19	1.04	1.13	1

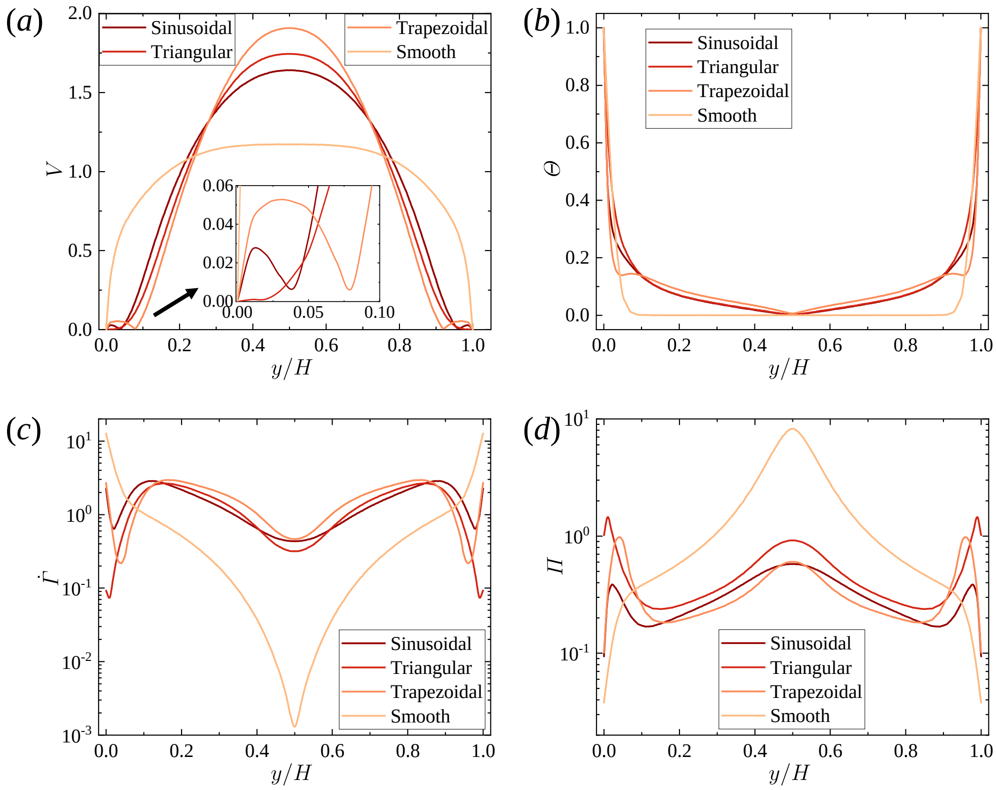

Figure 8. Profiles of the dimensionless (**a**) velocity, (**b**) temperature, (**c**) shear rate and (**d**) viscosity in the transverse direction at the outlet of the test section for smooth channel and channel with different corrugation profiles. The geometry and the flow conditions are listed in Table 3.

4.2. Effect of Wavelength L_w

In this section, five different wavelengths are chosen to investigate their effects on the gel flow. The length of the test section remains constant at $12H$. The number of the waves vary from 2 to 6. Thus, the wavelengths are $6H$, $5H$, $4H$, $3H$, $2.4H$ and $2H$, respectively. The simulation conditions are listed in Table 3.

The dimensionless velocity, temperature, shear rate and viscosity in the transverse direction at the outlet of the test section for different wavelengths are shown in Figure 9. From Figure 9a, it can be observed that a longer wavelength, L_w, leads to a blunter velocity profile. Figure 9b indicates that the temperature of the main flow is higher for a shorter length, L_w, because in the corrugation with shorter wavelengths, the flow recirculation is stronger. Thus, the heat convection is also stronger. Figure 9c indicates that overall, a shorter wavelength corresponds to a greater shear rate, except in the recirculation region. From Figure 9d, we can see that in the main flow, the viscosity of the gel is lower due to the higher temperatures when the wavelength is shorter. In the recirculation region, the pattern is not clear as the viscosity is determined by both the temperature and the shear rate.

Figure 10 shows the mean apparent viscosity at the outlet of the test section ($\overline{\Pi}$) and the dimensionless pressure drop of the test section (ΔP) for different L_w. It can be seen that the ΔP decreases as L_w increases, and the ΔP for $L_\mathrm{w} = 2H$ is almost twice the value for the case of $L_\mathrm{w} = 6H$. In the last section of the channel, we find that in the smooth channel, which can be treated as the situation of infinite L_w, ΔP is approximately 1. The viscous dissipation caused by the flow recirculation in the corrugations leads to an increase in the pressure drop. Despite the disadvantage of the increased ΔP, the existence of the recirculation regions not only enhances the heat transfer but also strengthens the shear stress, both of which are beneficial for the viscosity reduction. Figure 10 indicates that $\overline{\Pi}$ increases significantly with an increase in L_w.

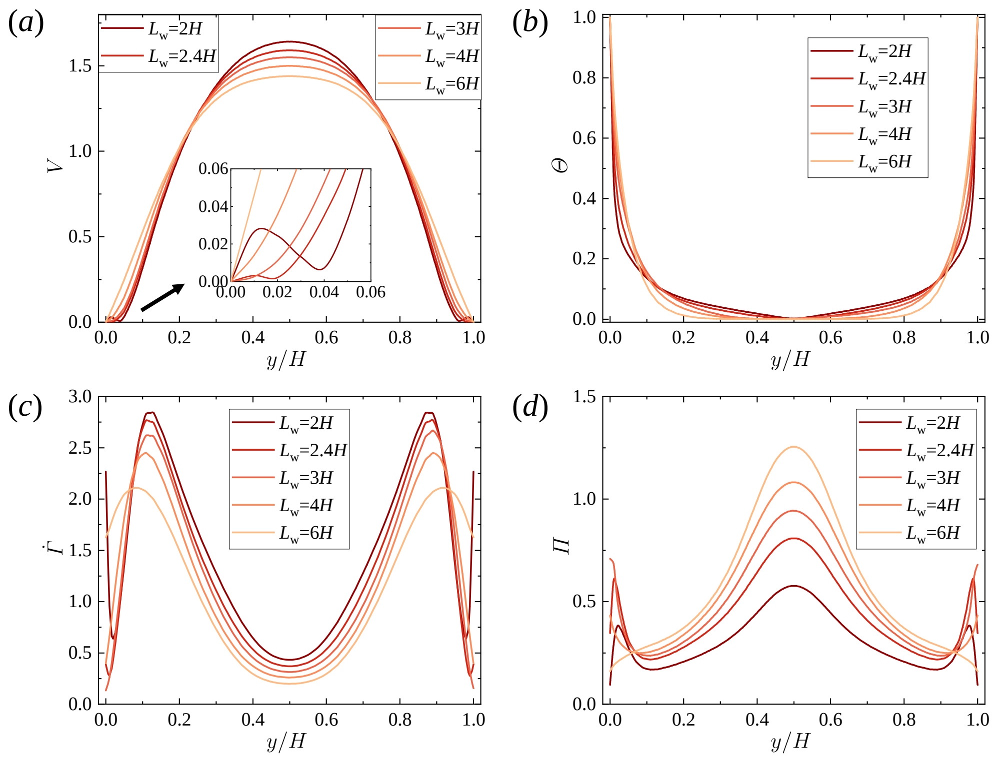

Figure 9. Profiles of the dimensionless (**a**) velocity, (**b**) temperature, (**c**) shear rate and (**d**) viscosity in the transverse direction at the outlet of test section for different wavelengths. The amplitude of the wave is $1/5H$, and $Re_{\text{gen,CY}}$ is 130.

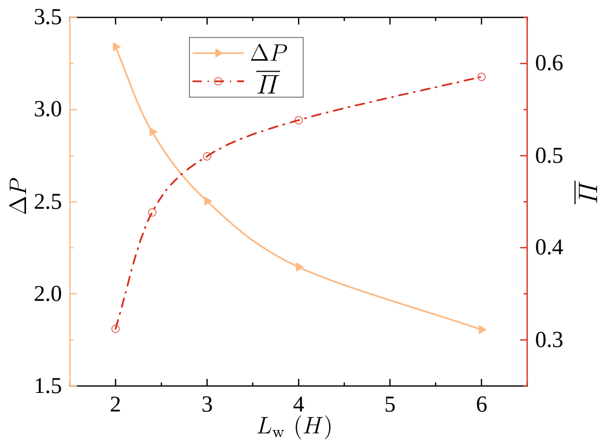

Figure 10. Mean apparent viscosity at the outlet of the test section ($\overline{\Pi}$) and dimensionless pressure drop of the test section (ΔP) for different L_{w}. The amplitude of the wave is $1/5H$, and $Re_{\text{gen,CY}}$ is 130.

4.3. Effect of Wave Amplitude a

In this part, we look at the influence of different wave amplitudes, a, on the gel flow. Five different amplitudes varying from $a = 0$ to $1/5H$ are studied, where $a = 0$ represents a smooth channel. The geometric properties of these five different configurations are presented in Table 3.

Figure 11 shows the dimensionless velocity, temperature, shear rate and viscosity in the transverse direction at the outlet of the test section for different wave amplitudes. Figure 11a indicates that a small amplitude leads to a blunter velocity profile, and near the wall, the recirculation region appears only when $a = 1/5H$. In terms of heat transfer, from Figure 11b, we can see that a larger amplitude produces a stronger heat exchange with flow.

Figure 11c shows that the corrugation changes the distribution of the shear rate where the variation of the shear rate profile becomes more moderate. In Figure 11d, we can see that a larger amplitude tends to reduce the viscosity of the gel in the main flow.

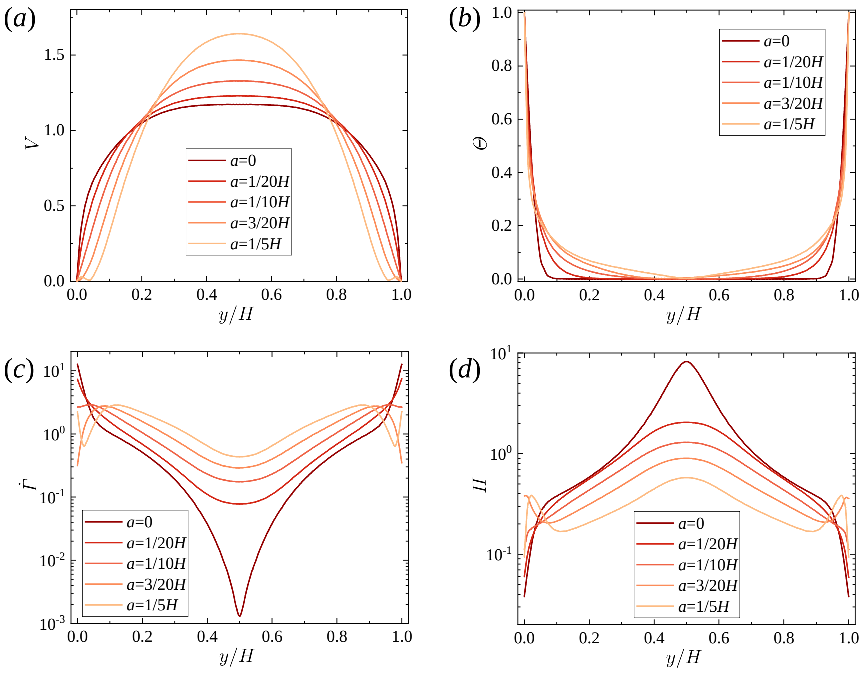

Figure 11. Profiles of the dimensionless (**a**) velocity, (**b**) temperature, (**c**) shear rate and (**d**) viscosity in the transverse direction at the outlet of test section for different wave amplitudes. The length of the wave is $2H$, and $Re_{\mathrm{gen,CY}}$ is 130.

Figure 12 shows the mean apparent viscosity ($\overline{\Pi}$) at the outlet of the test section and the dimensionless pressure drop of the test section (ΔP) for different wave amplitudes. We can see that ΔP increases with increasing wave amplitudes. The larger the wave amplitude, the faster the ΔP increases. In terms of the mean apparent viscosity, the difference between the smooth channel and the corrugated channels varied significantly. We notice that $\overline{\Pi}$ for $a = 1/20H$ is only half of that in the smooth channel. Among the corrugations with different amplitudes, the decrease in $\overline{\Pi}$ seems to have a linear relationship when the amplitude increases.

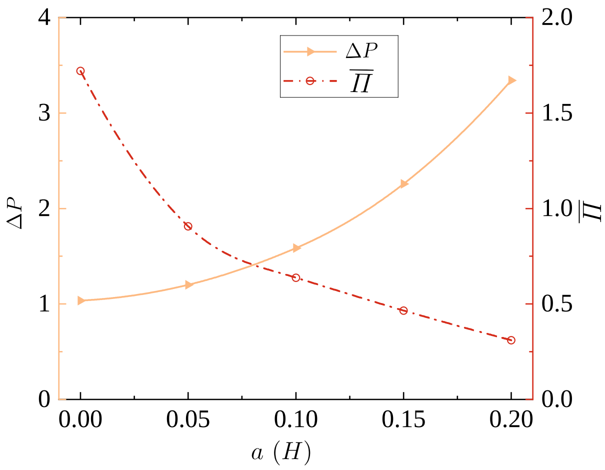

Figure 12. Mean apparent viscosity at the outlet of the test section ($\overline{\Pi}$) and dimensionless pressure drop of the test section (ΔP) for different wave amplitudes. The length of the wave is $2H$, and $Re_{\mathrm{gen,CY}}$ is 130.

4.4. Effect of the Reynolds Number $Re_{gen,CY}$

Here, we investigate the effect of the Reynolds number. The values used for the $Re_{\text{gen,CY}}$ (see Equation (14) for the definition) range from 43 to 555. The wavelength of the sinusoidal corrugation is $2H$, and the wave amplitude is $1/5H$.

Figure 13 shows the profiles for the dimensionless velocity, temperature, shear rate and viscosity for different values of $Re_{\text{gen,CY}}$. From Figure 13a, it can be seen that when the Reynolds number increases, the size of the recirculation regions grow. Interestingly, a larger Reynolds number and thus a larger recirculation region leads to a weaker thermal penetration into the main flow (see Figure 13b). Due to the change of the recirculation region, as seen in Figure 13c, the pattern of the shear rate near the wall also changes dramatically. From Figure 13d, we can see that the viscosity decreases as the $Re_{\text{gen,CY}}$ increases; this may be attributed to the enhanced effect of shear thinning. Figure 14 shows the mean apparent viscosity ($\overline{\Pi}$) at the outlet of the test section and the dimensionless pressure drop of the test section (ΔP) for different $Re_{\text{gen,CY}}$. As shown in Figure 14, both ΔP and $\overline{\Pi}$ decrease when the Reynolds number increases.

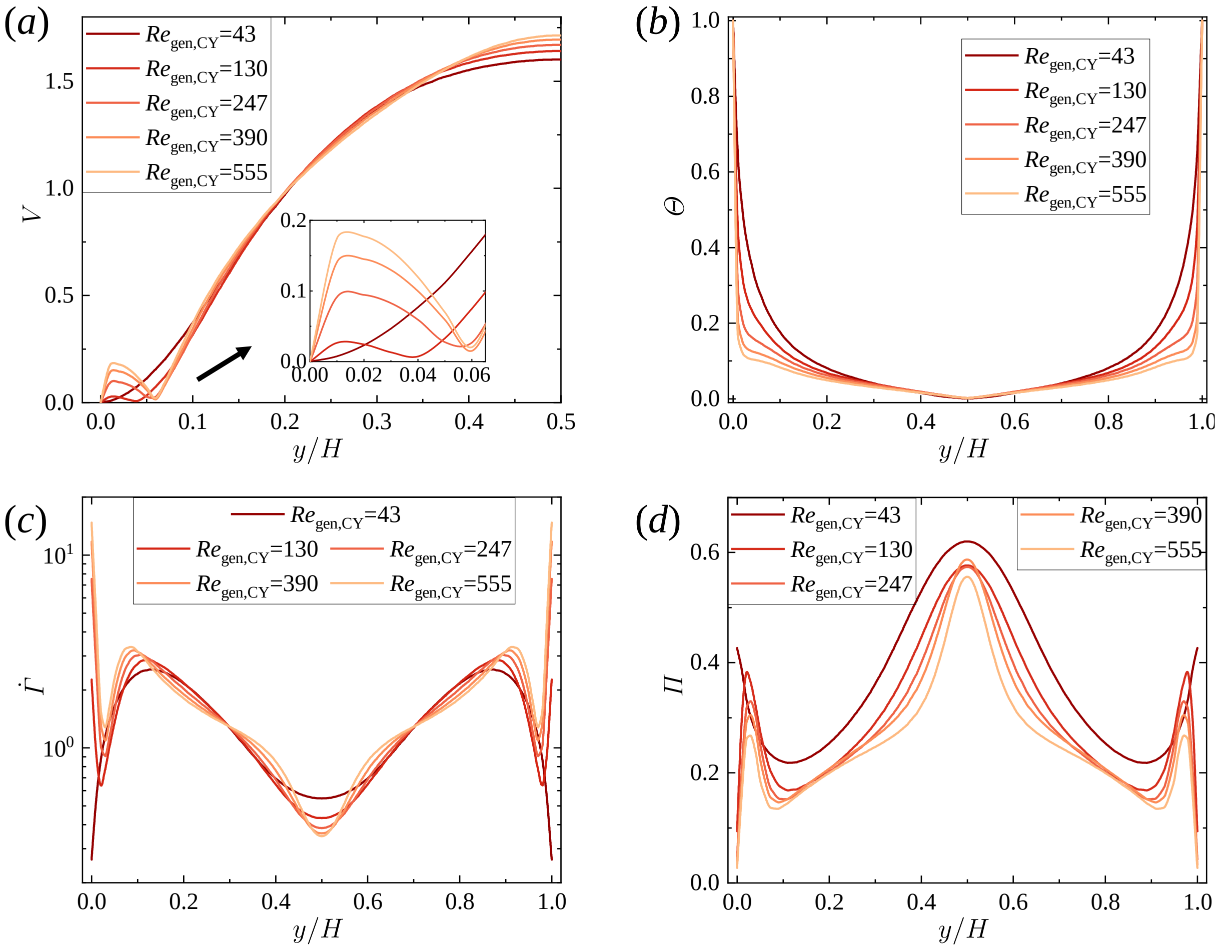

Figure 13. Profiles of the dimensionless (**a**) velocity, (**b**) temperature, (**c**) shear rate and (**d**) viscosity for different $Re_{\text{gen,CY}}$. The wavelength of the sinusoidal corrugation is $2H$, and the wave amplitude is $1/5H$.

4.5. Flow and Heat Transfer in a Y-Shape Corrugated Pipe

The purpose of introducing corrugation is to enhance the mixing of the flow and thus improving the heat convection in the pipe. A Y-shape channel, which is able to cause flow disturbance and mixing, has a similar function [43]. Therefore, we propose using a Y-shape corrugated pipe for investigating the viscosity reduction due to temperature changes, see Figure 15a. The Y-shape corrugated pipe has two inlets with a diameter H. The corrugation part has a similar configuration as the case in Section 4.4. The diameter of the outlet is $\sqrt{2}H$. Two inlet velocity conditions are studied: a constant inlet velocity condition, $V_{\text{in1}} = V_{\text{in2}} = V_0$, and a pulsed inlet velocity condition, which is defined by the following equations:

$$\begin{aligned} V_{\text{in1}} &= V_0(1 + M_p sin(2\pi f t)) \\ V_{\text{in2}} &= V_0(1 + M_p \sin(2\pi f t + \pi)) \end{aligned} \tag{24}$$

where V_{in1} and V_{in2} are the applied velocities at the two inlets, V_0 is the mean inlet velocity, f is the pulsation frequency, and M_p is the amplitude. From the above equations, it can be seen that for the pulsed case, the outlet velocity is constant. In this case, we choose $M_p = 1$, $f = 10$ Hz, and the Reynolds number (using V_0 as the reference velocity) is 130.

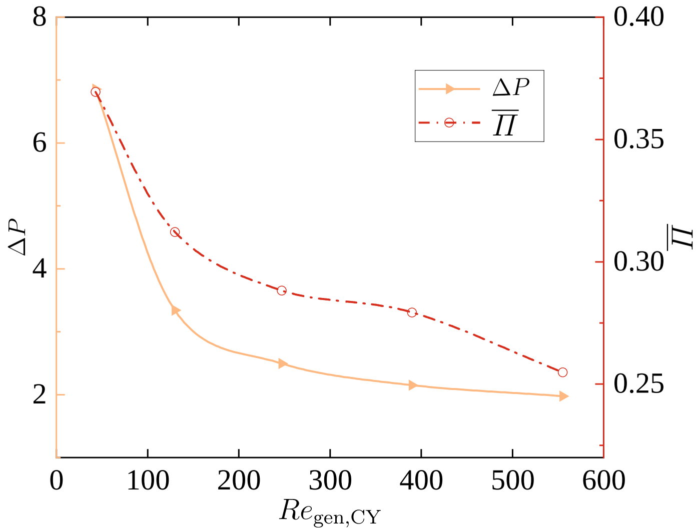

Figure 14. Mean apparent viscosity at the outlet of the test section ($\overline{\Pi}$) and the dimensionless pressure drop of the test section (ΔP) for different $Re_{\text{gen,CY}}$. The length of the wave is $2H$, and the amplitude of the wave is $1/5H$.

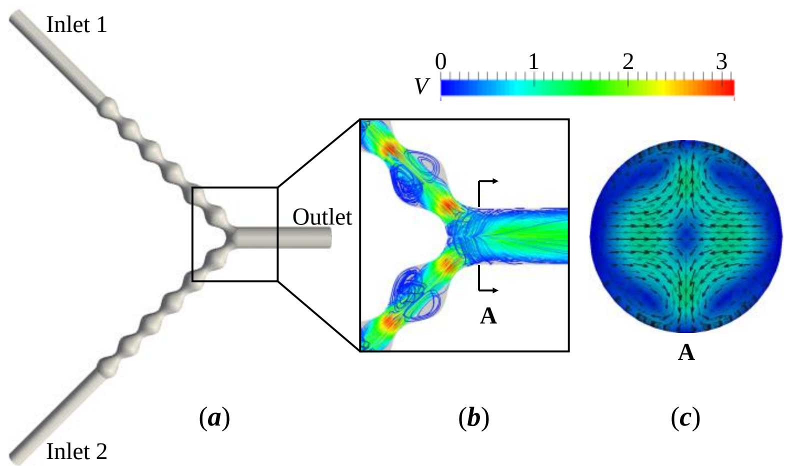

Figure 15. (**a**) Geometry of the 3D Y-shape corrugated pipe, (**b**) streamlines near the intersection of the two corrugated pipes and (**c**) the velocity vector in cross section A when $V_{\text{in1}} = V_{\text{in2}}$.

Figure 15b shows the streamlines near the intersection of the two corrugated pipes when $V_{\text{in1}} = V_{\text{in2}}$. Clearly, flow recirculations can be noticed in the corrugations, and a strong mixing can be observed in the intersection region of the two corrugated pipes, which is indicated by the velocity vector field shown in Figure 15c. Figure 16 shows the evolution of the dimensionless velocity fields in one pulse period. The inlet velocity is controlled by Equation (24). We can see an obvious disturbance on the velocity fields, which can cause the gel in the pipe (after the intersection) be mixed adequately (see Figure 17 for the dimensionless temperature field as the indication of the well mixing). Comparing the temperature fields before and after the intersection, as shown in Figure 17, we can see that in the corrugated channel, the temperature difference between the main flow and near the wall region is much more noticeable than the region after the intersection.

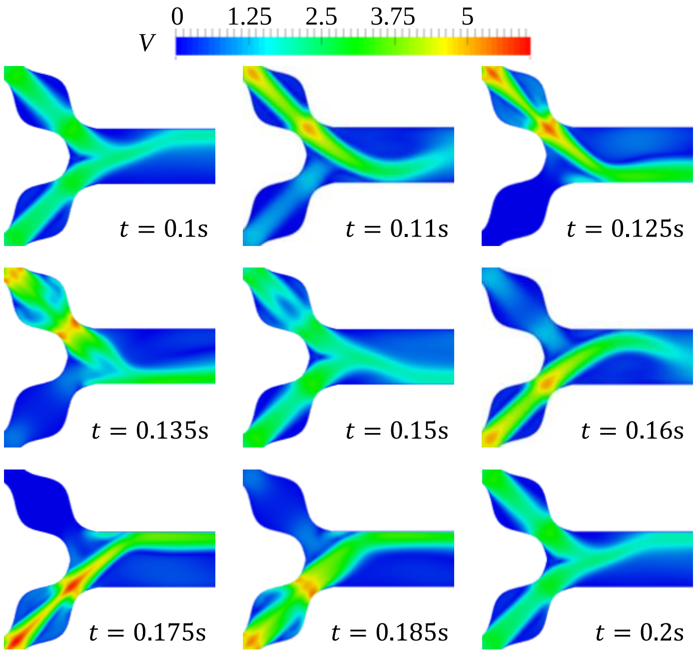

Figure 16. Evolution of the velocity field during one pulse period.

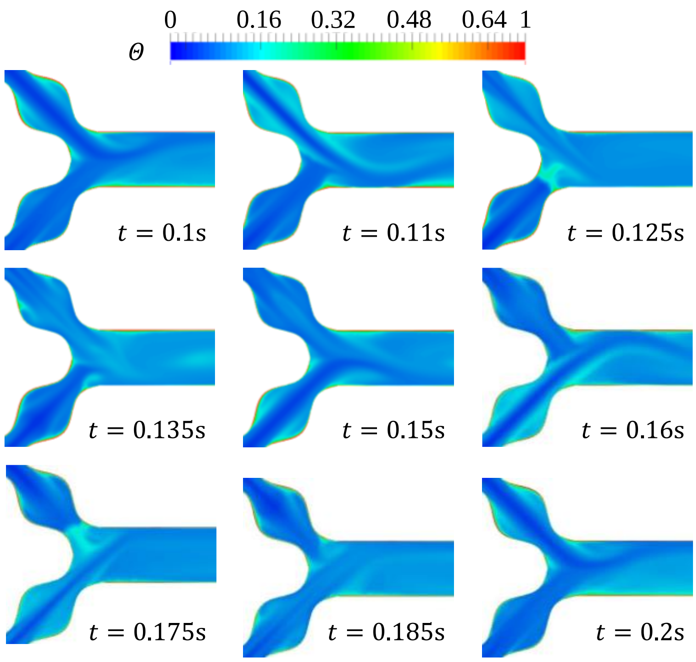

Figure 17. Evolution of temperature field during one pulse period.

Figure 18 shows the dimensionless mean and the transient apparent viscosity in one pulse period. The apparent viscosity of water at $\Theta = 0$ is considered as the reference viscosity in this case. In Figure 18, the red dash line represents the dimensionless mean apparent viscosity which is constant ($\overline{\Pi} = 81$), when the applied inlet velocity is $V_{\text{in1}} = V_{\text{in2}} = V_0$.

For the pulse inlet velocity, the mean apparent viscosity changes semi-periodically, and the time-averaged dimensionless mean apparent viscosity is $\overline{\Pi} = 76$. For comparison, the mean apparent viscosity in a smooth pipe is calculated, and the resulting dimensionless mean apparent viscosity is $\overline{\Pi} = 277.5$. Therefore, compared with a smooth straight pipe, the Y-shape corrugated pipe provides a decrease of 70.8% for the mean apparent viscosity, and the viscosity reduction percentage becomes 72.6% when a pulse inlet velocity is applied.

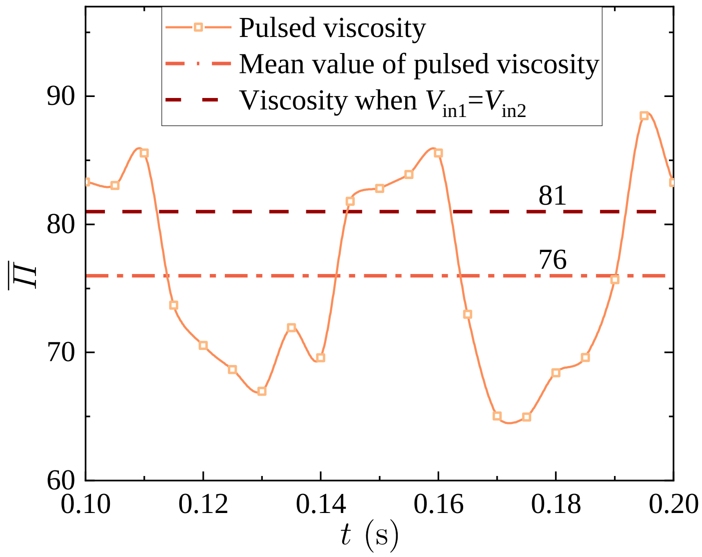

Figure 18. Mean apparent viscosity at cross section A in the Y-shape corrugated channel with pulsed and constant inlet velocity conditions.

5. Conclusions

In this paper, we investigate the heat transfer and flow of a gel fuel (mimicked by water-gel) in corrugated channels. We focus on the effect of the corrugation and temperature on the viscosity reduction of the gel, which is essential for the spray atomization and combustion for a propulsion system using gel fuel. The Carreau-Yasuda (shear-thinning) equation combined with the Andrade-Eyring (temperature-sensitive) viscosity model is used to describe the temperature and the shear sensitive viscosity of the gel. The constitutive parameters are fitted with the available experimental data. We also perform parametric studies for different corrugation configurations and flow conditions to investigate the impact on the pressure drop and the viscosity reduction. According to the numerical results, we can draw the following conclusions:

1. The recirculation regions generated by the corrugations enhance the heat convection and are beneficial for reducing the viscosity, while simultaneously the pressure drop seems to increase due to the viscous dissipation caused by the circulation. For different corrugation profiles, the sinusoidal corrugation can achieve lower viscosity with a lower pressure drop compared with the triangular and the trapezoidal corrugations.
2. For the sinusoidal corrugation, a shorter wavelength and a deeper wave amplitude seem to be better for reducing the viscosity, but it also has the adverse consequence of the increased pressure drop. Furthermore, in the range of the parameters studied in this paper, a larger Reynolds number is more desirable for both lowering the pressure drop and reducing the viscosity.
3. Compared with a smooth straight pipe, a Y-shape corrugated pipe with a constant inlet velocity can reduce the mean apparent viscosity by 70.8%, going up to 72.6% if a pulse inlet velocity is applied; this can significantly enhance the gel fuel atomization and thus improve the combustion efficiency.
4. In terms of practical significance, compared with straight pipes, corrugated pipes with heated walls can effectively reduce the apparent viscosity of the gel at the outlet of

the pipe, which will further facilitate the atomization of the gel. This has significant application prospects in propulsion processes using kerosene gel as fuel.

5. For future work, we mention that the current paper mainly studies the viscosity reduction in gels due to temperature variations. From the conclusion, it can be seen that the effect is very significant. The working conditions and the overall composition of the pipeline are also different from the actual propulsion systems. The next step should be to carry out research on the actual engineering conditions and pipeline structure and explore the effects of viscosity reduction at the engineering application level.

Author Contributions: H.Z. and Q.-L.C. performed the simulations. C.Z., W.-T.W. and M.M. supervised the work. All the authors contributed to the manuscript writing. F.F. and H.Z. contributed to this paper equally. All authors have read and agreed to the published version of the manuscript.

Funding: This work is supported by Natural Science Foundation of China No. 11802135 and the Fundamental Research Funds for the Central Universities No. 30919011401.

Conflicts of Interest: The authors declare no conflict of interest.

References

1. Ciezki, H.K.; Hürttlen, J.; Naumann, K.W.; Negri, M.; Ramsel, J.; Weiser, V. Overview of the German Gel Propulsion Technology. In Proceedings of the 50th AIAA/ASME/SAE/ASEE Joint Propulsion Conference, Cleveland, OH, USA, 28–30 July 2014; pp. 1–16.
2. Arnold, R.; Anderson, W. Droplet burning of JP-8/Silica gels. In Proceedings of the 48th AIAA Aerospace Sciences Meeting Including the New Horizons Forum and Aerospace Exposition, Orlando, FL, USA, 4–7 January 2010; pp. 1–12.
3. Ciezki, H.K.; Naumann, K.W.; Weiser, V. Status of Gel Propulsion in the Year 2010 with a Special View on the German Activities. In Proceedings of the Deutschland Luft-und Raumfahrtkongress, Hamburg, Germany, 31 August–29 September 2010.
4. Natan, B.; Rahimi, S. The status of gel propellants in year 2000. *Int. J. Energ. Mater. Chem. Propuls.* **2002**, *5*, 172–194. [CrossRef]
5. Gafni, G.; Kuznetsov, A.; Har-Lev, D.; Natan, B. Experimental Investigation of a Ramjet Combustor Using an Aluminized Gel Fuel. In Proceedings of the 49th AIAA/ASME/SAE/ASEE Joint PropulsionConference, San Jose, CA, USA, 14–17 July 2013; p. 3748.
6. Matsibeker, E.; Natan, B. Numerical Solution of the Flowfield in an Aluminized Gel Fuel Ramjet. In Proceedings of the 49th AIAA/ASME/SAE/ASEE Joint Propulsion Conference, San Jose, CA, USA, 14–17 July 2013; p. 3976.
7. Natan, B.; Haddad, A.; Arieli, R. Performance assessments of a boron containing gel fuel ramjet. In Proceedings of the 47th AIAA Aerospace Sciences Meeting Including the New Horizons Forum and Aerospace Exposition, Orlando, FL, USA, 5–8 January 2009; p. 1421.
8. Doi, M. Explanation for the 3.4-power law for viscosity of polymeric liquids on the basis of the tube model. *J. Polym. Sci. Polym. Phys. Ed.* **1983**, *21*, 667–684. [CrossRef]
9. Doi, M. Explanation for the 3.4-power law of viscosity of polymeric liquids on the basis of the tube model. *J. Polym. Sci. Polym. Lett. Ed.* **1981**, *19*, 265–273. [CrossRef]
10. Krieger, I.M. Rheology of monodisperse latices. *Adv. Colloid Interface Sci.* **1972**, *3*, 111–136. [CrossRef]
11. Rahimi, S.; Natan, B. Numerical solution of the flow of power-law gel propellants in converging injectors. *Propellants Explos. Pyrotech.* **2000**, *25*, 203–212. [CrossRef]
12. Rahimi, S.; Natant, B. The injection process of gel fuels. In Proceedings of the 33rd Joint Propulsion Conference and Exhibit, Seattle, WA, USA, 6–9 July 1997.
13. Rahimi, S.; Natan, B. Flow of Gel Fuels in Tapered Injectors. *J. Propuls. Power* **2000**, *16*, 458–464. [CrossRef]
14. Yoon, C.; Heister, S.D.; Xia, G.; Merkle, C.L. Numerical modeling of injection of shear-thinning gel propellants through plain-orifice atomizer. *J. Propuls. Power* **2011**, *27*, 944–954. [CrossRef]
15. Cao, Q.-L.; Massoudi, M.; Liao, W.-H.; Feng, F.; Wu, W.-T. Flow Characteristics of Water-HPC Gel in Converging Tubes and Tapered Injectors. *Energies* **2019**, *12*, 1643. [CrossRef]
16. Middleman, S. *Fundamentals of Polymer Processing*; McGraw-Hill: New York, NY, USA, 1977.
17. Carreau, P.J.; De Kee, D.; Chhabra, R.J. *Rheology of Polymeric Systems*; Hanser/Gardner Publications: Cincinnati, OH, USA, 1997.
18. Shin, S.; Cho, Y.I. Laminar heat transfer in a rectangular duct with a non-Newtonian fluid with temperature-dependent viscosity. *Int. J. Heat Mass Transf.* **1994**, *37*, 19–30. [CrossRef]
19. Rahimi, S.; Peretz, A.; Natan, B. Rheological matching of gel propellants. *J. Propuls. Power* **2010**, *26*, 376–379. [CrossRef]
20. Rahimi, S.; Natan, B. Atomization characteristics of gel fuels. In Proceedings of the 34th AIAA/ASME/SAE/ASEE Joint Propulsion Conference and Exhibit, Cleveland, OH, USA, 13–15 July 1998; p. 3830.
21. Cao, Q.L.; Wu, W.T.; Liao, W.H.; Feng, F.; Massoudi, M. Effects of temperature on the flow and heat transfer in gel fuels: A numerical study. *Energies* **2020**, *13*, 821. [CrossRef]
22. Kareem, Z.S.; Jaafar, M.N.M.; Lazim, T.M.; Abdullah, S.; Abdulwahid, A.F. Passive heat transfer enhancement review in corrugation. *Exp. Therm. Fluid Sci.* **2015**, *68*, 22–38. [CrossRef]

23. Hong, Y.; Du, J.; Wang, S.; Huang, S.-M. Heat transfer and flow behaviors of a wavy corrugated tube. *Appl. Therm. Eng.* **2017**, *126*, 151–166. [CrossRef]
24. Akbarzadeh, M.; Rashidi, S.; Esfahani, J.A. Influences of corrugation profiles on entropy generation, heat transfer, pressure drop, and performance in a wavy channel. *Appl. Therm. Eng.* **2017**, *116*, 278–291. [CrossRef]
25. Wang, W.; Zhang, Y.; Li, Y.; Han, H.; Li, B. Numerical study on fully-developed turbulent flow and heat transfer in inward corrugated tubes with double-objective optimization. *Int. J. Heat Mass Transf.* **2018**, *120*, 782–792. [CrossRef]
26. Saikia, A.; Dalal, A.; Pati, S. Thermo-hydraulic transport characteristics of non-Newtonian fluid flows through corrugated channels. *Int. J. Therm. Sci.* **2018**, *129*, 201–208.
27. Afrouzi, H.H.; Ahmadian, M.; Moshfegh, A.; Toghraie, D.; Javadzadegan, A. Statistical analysis of pulsating non-Newtonian flow in a corrugated channel using Lattice-Boltzmann method. *Phys. A Stat. Mech. Appl.* **2019**, *535*, 122486. [CrossRef]
28. Hilo, A.K.; Talib, A.R.A.; Iborra, A.A.; Sultan, M.T.H.; Hamid, M.F.A. Effect of corrugated wall combined with backward-facing step channel on fluid flow and heat transfer. *Energy* **2020**, *190*, 116294. [CrossRef]
29. Wu, W.T.; Aubry, N.; Massoudi, M. Flow of granular materials modeled as a non-linear fluid. *Mech. Res. Commun.* **2013**, *52*, 62–68. [CrossRef]
30. Slattery, J.C. *Advanced Transport Phenomena*; Cambridge University Press: Cambridge, UK, 1999.
31. Winterton, R.H.S. Early study of heat transfer: Newton and Fourier. *Heat Transf. Eng.* **2001**, *22*, 3–11. [CrossRef]
32. Zhang, M.; Che, Z.; Chen, J.; Zhao, H.; Yang, L.; Zhong, Z.; Lu, J. Experimental Determination of Thermal Conductivity of Water–Agar Gel at Different Concentrations and Temperature. *J. Chem. Eng. Data* **2010**, *56*, 859–864. [CrossRef]
33. Macosko, C.W.; Larson, R.G. *Rheology: Principles, Measurements, and Applications*; Wiley-VCH: Weinheim, Germany, 1994.
34. Bird, R.B.; Curtiss, C.F.; Armstrong, R.C.; Hassager, O. *Dynamics of Polymeric Liquids: Volume 2: Kinetic Theory*; John Wiley & Sons: Hoboken, NJ, USA, 1987.
35. Arnold, R.; Anderson, W.; Santos, P.H.S.; de Ridder, M.; Campanella, O.H. Comparison of Monomethylhydrazine/hydroxypropylcellulose and Hydrocarbon/silica Gels. In Proceedings of the 48th AIAA Aerospace Sciences Meeting Including the New Horizons Forum and Aerospace Exposition, Orlando, FL, USA, 4–7 January 2010; p. 422.
36. Miao, L.; Massoudi, M. Heat transfer analysis and flow of a slag-type fluid: Effects of variable thermal conductivity and viscosity. *Int. J. Non-Linear Mech.* **2015**, *76*, 8–19. [CrossRef]
37. Miao, L.; Massoudi, M. Effects of shear dependent viscosity and variable thermal conductivity on the flow and heat transfer in a slurry. *Energies* **2015**, *8*, 11546–11574. [CrossRef]
38. Szeri, A.Z. *Fluid Film Lubrication: Theory and Design*; Cambridge University Press: Cambridge, UK, 1998.
39. Massoudi, M.; Christie, I. Effects of variable viscosity and viscous dissipation on the flow of a third grade fluid in a pipe. *Int. J. Non-Linear Mech.* **1995**, *30*, 687–699. [CrossRef]
40. *OpenFOAM Programmer's Guide*; Version 2.1.0; OpenCFD: Bracknell, UK, 2011.
41. Rahimi, S.; Peretz, A.; Natan, B. On Shear Rheology of Gel Propellants. *Propellants Explos. Pyrotech.* **2010**, *32*, 165–174. [CrossRef]
42. Siebert, M.W.; Fodor, P.S. Newtonian and non-newtonian blood flow over a backward-facing step—A case study. In Proceedings of the COMSOL Conference, Boston, MA, USA, 8–10 October 2009.
43. Wu, W.-T.; Massoudi, M.; Yan, H. Heat transfer and flow of nanofluids in a Y-type intersection channel with multiple pulsations: A numerical study. *Energies* **2017**, *10*, 492. [CrossRef]